Towards chemical validation of *Leishmania infantum* ribose 5-phosphate isomerase as a drug target

Emily A. Dickie[a], **Céline Ronin**[b], Mónica Sá[c,d], Fabrice Ciesielski[b], Nathalie Trouche[b], Joana Tavares[c,d], Nuno Santarem[c,d], Louise L. Major[a], Iain K. Pemberton[e], Jane MacDougall[e], Terry K. Smith[a#], Anabela Cordeiro-da-Silva[c,d,f#] & Paola Ciapetti[b#]

[a]Biomedical Sciences Research Complex, University of St. Andrews, St Andrews, Fife, Scotland, UK;

[b]NovAliX, Biology Department, Illkirch Cedex, France

[c]i3S–Instituto de Investigação e Inovação em Saúde, Universidade do Porto, Porto, Portugal;

[d]IBMC-Instituto de Biologia Molecular e Celular, Parasite Disease Group, Porto, Portugal;

[e]Photeomix Protein Discovery, IP Research Consulting, Noisy Le Grand, France;

[f]Departmento de Ciências Biológicas, Faculdade de Farmácia, Universidade do Porto, Porto, Portugal.

[#]Joint corresponding authors: Terry K. Smith, tks1@st-andrews.ac.uk

Paola Ciapetti, pciapetti@novalix.com

Anabela Cordeiro da Silva, cordeiro@ibmc.up.pt

Antimicrobial Agents and Chemotherapy

22 Running title: *L. infantum* RpiB screening and structure

23 Keywords: Neglected tropical diseases, *Leishmania infantum*, leishmaniasis, ribose
24 5-phosphate isomerase, inhibitor, screening, thermal shift, anti-parasitic, protein
25 crystal structure

26

Abstract

Neglected tropical diseases caused by kinetoplastid parasites (*Trypanosoma brucei*, *Trypanosoma cruzi* and *Leishmania* spp.) place a significant health and economic burden on developing nations worldwide. Current therapies are largely out-dated, inadequate and facing mounting drug resistance from the causative parasites. Thus, there is an urgent need for drug discovery and development. Target-led drug discovery approaches have focused on the identification of parasite enzymes catalysing essential biochemical processes, which significantly differ from equivalent proteins found in humans, thereby providing potentially exploitable therapeutic windows. One such target is ribose 5-phosphate isomerase B (RpiB), an enzyme involved in the non-oxidative branch of the pentose phosphate pathway, which catalyses the inter-conversion of D-ribose 5-phosphate and D-ribulose 5-phosphate. Although protozoan RpiB has been the focus of numerous targeted studies, compounds capable of selectively inhibiting this parasite enzyme have not been identified. Here, we present the results of a fragment library screening against *Leishmania infantum* RpiB, performed using thermal shift analysis. Hit fragments were shown to be effective inhibitors of *Li*RpiB in activity assays, and several were capable of selectively inhibiting parasite growth *in vitro*. These results support the identification of *Li*RpiB as a validated therapeutic target. The X-ray crystal structure of apo *Li*RpiB was also solved, permitting docking studies to assess how hit fragments might interact with *Li*RpiB to inhibit its activity. Overall, this work will guide structure-based development of *Li*RpiB inhibitors as anti-leishmanial agents.

52 **Introduction**

53

54 The kinetoplastid protozoan parasites *Trypanosoma brucei*, *Trypanosoma cruzi* and
55 *Leishmania* spp. are causative agents of the neglected tropical diseases (NTDs)
56 human African trypanosomiasis (HAT), Chagas disease and leishmaniasis
57 respectively. These NTDs continue to have a hugely damaging impact on global
58 health and economies, yet currently available chemotherapeutic options are widely
59 inadequate, and no effective human vaccines are available. Although significant
60 progress has been made in recent years (1), particularly in the treatment of HAT (2),
61 it has remained challenging to develop new drugs for leishmaniasis. Cutaneous
62 leishmaniasis (CL) and visceral leishmaniasis (VL) pose a major health threat to an
63 estimated 1 billion people, with over 1 million cases occurring annually, VL causing
64 20,000-30,000 deaths (3, 4). Although a number of therapeutic candidates are
65 progressing into clinical trials (5), most are at early stages and further leads are
66 required to off-set the often high attrition rates of clinical development. This is
67 particularly true in the case of leishmaniasis where treatment complexity is
68 heightened by the requirements of different regions, which experience infections
69 driven by different leishmanial species that also exhibit differing drug susceptibilities.
70 Thus, sustained efforts to identify new avenues for anti-leishmanial lead discovery
71 are vital. This need has led to extensive research into the metabolism of *Leishmania*
72 spp. parasites, with a view to establishing areas of biochemical divergence from their
73 hosts that can be exploited to combat them whilst minimising potential side-effects.
74

75 The enzyme ribose-5-phosphate isomerase (Rpi) catalyses the isomerization of
76 ribose-5-phosphate (R5P) to ribulose-5-phosphate (Ru5P) (Figure S1) in the non-

oxidative branch of the pentose phosphate pathway (PPP) (Figure 1) (6, 7). Alongside glycolysis and the Kreb's cycle, the PPP was one of the first identified metabolic pathways and is highly conserved in both prokaryotes and eukaryotes (8). The PPP supports key cellular functions, with the non-oxidative branch providing precursors for nucleotide, amino acid and vitamin biosynthesis, and the oxidative branch contributing to redox regulation (8). Though the oxidative branch of the pathway is confined to eukaryotes, the non-oxidative pathway is common to all organisms. Two physically and genetically distinct forms of Rpi are known to exist and were first characterised in *Escherichia coli* K12 (9), which produces both types. RpiA is present in all taxonomic groups but RpiB has only been found in bacteria and lower eukaryotes, including protozoa (10).

The fact RpiBs are found exclusively in lower eukaryotes, including human pathogenic species, has led to them becoming the focus of numerous studies aiming to establish their essentiality, solving their protein structure and identifying specific inhibitors. Crystal structures for the RpiBs from *E. coli* and *Mycobacterium tuberculosis* have been determined to facilitate targeted drug design (11–13). Inhibition studies have centred on mimicking the structure of the high energy *cis*-enediolate isomerisation reaction intermediate, such that inhibitors including 4-phospho-D-erythronohydroxamic acid (4-PEH) have been identified (14). However, these inhibitors lack selectivity for RpiBs, given RpiAs also catalyse isomerisation via this high-energy intermediate, meaning they are unlikely to provide routes to the development of novel, selective therapeutics.

The RpiBs from kinetoplastid parasites have also been examined. RpiB downregulation through RNA interference (RNAi) in *T. brucei* decreased parasite *in*

Antimicrobial Agents and Chemotherapy

vitro growth and the infectivity of bloodstream forms towards mice (15). Mice infected with induced RNAi clones exhibited lower parasitaemia and a prolonged survival compared to control mice. Phenotypic reversion was achieved by complementing induced RNAi clones with an ectopic copy of the *Trypanosoma cruzi* gene (15). A crystal structure for *T. cruzi* RpiB (*Tc*RpiB) has been determined (16), and research into the enzyme's substrate specificity and potential inhibition has been conducted (17). *Leishmania spp.* RpiB has been studied in *Leishmania donovani*, *Leishmania major* and *Leishmania infantum* (10, 18, 19). In *L. infantum* null mutant generation was only possible when an episomal copy of the RpiB gene was provided, and the latter was preserved both *in vitro* and *in vivo* in the absence of drug pressure. This indicates the gene is essential for parasite survival (19). Although kinetoplastid RpiBs have also been shown to be susceptible to 4-PEH inhibition, no other specific inhibitors have yet been identified, potentially as studies of these enzymes have been largely dominated by structural modelling and *in silico* inhibition prediction (10, 20).

Here, we present the findings from a thermal shift (differential scanning fluorimetry) fragment library screening against recombinantly expressed *L. infantum* RpiB (*Li*RpiB). Hits obtained were analysed for their ability to inhibit *Li*RpiB via *in vitro* activity assay and for their anti-parasitic potency in cell viability assays. Results indicate that ability to interact with and effectively inhibit *Li*RpiB can be linked to anti-parasitic efficacy, strengthening the case for *Li*RpiB as a validated drug target. We have also determined the first X-ray crystal structure for a *Leishmania* spp. RpiB, which permitted *in silico* docking analysis to speculate how the hit inhibitory fragments identified during this research might bind and inhibit *Li*RpiB activity.

Overall, this work provides novel insight that will inform the design of kinetoplastid RpiB-specific leads for drug development.

Results

*Li*RpiB recombinant protein was expressed, purified and subjected to thermal shift analysis. Thermal shift (differential scanning fluorimetry) is reliant on fluorescent dyes that signify when a protein has unfolded (21). One of the most commonly used fluorescent dyes is SYPRO® Orange (also used here), which forms non-specific interactions with hydrophobic protein residues (22). This means its signal will be strongest when the protein being analysed is unfolded and internal hydrophobic residues are exposed. By running an assay where reaction temperature is increased in degree increments per minute, it is possible to define the temperature at which a protein unfolds by monitoring its fluorescence. The temperature at which this occurs is designated the protein's (T_m) or melting point (21). Compounds that significantly alter T_m may be potential inhibitors. Initial testing showed *Li*RpiB was amenable to SYPRO® Orange thermal shift analysis, with an average T_m of 59.6°C being obtained for the protein.

To permit screening of a fragment library, a positive control for ligand binding had to be established. The obvious choice was the enzyme's substrate: ribose-5-phosphate (R5P). However, reported Km values for R5P against other RpiB enzymes were relatively high, with Stern et al. reporting a R5P Km of 4 mM against *Tc*RpiB (17). Indeed, no significant shifts in *Li*RpiB T_m in the presence of 5-50 mM R5P could be obtained, supporting the suggestion that R5P has a relatively weak interaction with *Li*RpiB and other parasitic RpiBs.

It was hypothesised that 2-deoxyribose-5-phosphate (dR5P) may serve as an alternative, as it could be sufficiently similar to R5P to bind *Li*RpiB but also be retained in the enzyme's active site for longer, prolonging the interaction. Testing a gradient of dR5P against *Li*RpiB (5-50 mM) resulted in significant shifts in *Li*RpiB T_m. To provide the consistency across replicates that would provide Z-factor values for each plate above the confidence threshold (Z-factor > 0.5), 30 mM was selected as the dR5P concentration for positive control reactions, reproducibly inducing a 6 °C shift in *Li*RpiB T_m (Figure 2).

Approximately 800 fragments (Figure S2) across 11 fragment plates (Z-factors ranging from 0.5 – 0.8) (Figure S3), were screened at 1 mM effective concentration against *Li*RpiB. Graphs to summarise the data output for each fragment plate were compiled, with change in T_m relative to the negative control represented for each individual fragment (Figure S4).

Upon reviewing the thermal shift data for the fragments, a threshold T_m shift of ± 5°C was set for fragment hit selection. This led to the selection of 15 fragment hits (Table 1), which were followed up with enzymatic assays and anti-parasitic activity studies.

Initially, fragment inhibition was tested in *Li*RpiB *in vitro* activity assays. Inhibition was compared to that achieved with the well-established Rpi inhibitor 4-PEH, which was tested at 10 mM concentration against both the forward (R5P -> Ru5P) and reverse (Ru5P -> R5P) isomerisation reactions (Table 2). Fragments 328 and 458 were excluded from these assays due to solubility problems. To assess whether fragments could be tested in the forward reaction assay, their absorbance at 290 nm

(0.5 mM and 1 mM concentration) was measured. Almost all fragments displayed high absorbance values at 290 nm (OD ≥ 1) (Figure S5). Therefore, they could not be tested in the forward Rpi activity assay.

Only fragments 2, 3, 25, 372, 540 and 576 were tested in this assay. Results for fragment 540 were also excluded during posterior analysis as, in the presence of R5P, the measured signal became saturated, which hindered a clear interpretation of the measurements obtained. Percentage inhibition values for *Li*RpiB that could be determined from the forward Rpi assay are shown (Table 2). No significant inhibition was found through this assay system except in the case of fragment 576: 1 mM 576 inhibited the forward reaction to a similar extent as 10 mM 4-PEH (Figure 3). This suggests that 576 is (at least) as potent an inhibitor of *Li*RpiB as 4-PEH.

The experimental limitations of the forward reaction assay do not apply to the reverse reaction assay. Therefore, all compounds could be tested in the reverse reaction assay system. Fragments 2, 338, 372 and 540 (1 mM) were capable of inhibiting the enzyme to a similar level as 10 mM 4-PEH (Table 2). Surprisingly, the inhibitory capacity of fragment 576 and 4-PEH were not as high in this assay system. This may be due to kinetoplastid RpiB activity favouring production of R5P, meaning higher levels of these inhibitors may be required in order to inhibit the enzyme in this direction.

The 15 fragment hits and 4-PEH were also tested for their ability to inhibit *L. infantum* parasite growth at 100 µM concentration. Compounds were assayed against both *L. infantum* promastigotes (wild-type and *Li*RpiB sKO) and intra-

198 macrophagic amastigotes (Table 2). As 4-PEH is only an inhibitor of LiRpiB at high
199 millimolar range in protein activity assays (10 mM was routinely used to achieve
200 inhibition during this study), it had been anticipated to show little to no anti-parasitic
201 activity *in vitro*/*in vivo* (7), which was shown to be the case in treating with 100 μM.
202 However, several of the fragment hits were shown to inhibit parasite growth at this
203 concentration. Interestingly, fragments 152, 278 and 540 were seemingly less
204 effective against the LiRpiB sKO promastigotes than the wild-type. Although sKO
205 modifications against essential genes often do not produce significant phenotypic
206 distinctions from wild-type parasites, it's possible that compensatory up-regulation
207 mechanisms accounting for the loss of a single *Li*RpiB allele are acting to protect the
208 parasites from treatment with these compounds (to some extent). Conversely,
209 fragment 576 was active against *Li*RpiB sKO promastigotes but was inactive against
210 the wild-type. As the *in vitro* enzyme assay results point to fragment 576 being a
211 more effective inhibitor of the *Li*RpiB forward reaction than the reverse reaction, this
212 could indicate sKO parasites are rendered more susceptible to forward reaction
213 inhibitors. The most active fragments against both *L-infantum* life-cycle forms were
214 338 (Figure 4) and 540, which were also among the most potent inhibitors of the
215 *Li*RpiB reverse reaction. Collectively, these data suggest that a possible mode of
216 action for the observed anti-leishmanial activity of potent fragments, such as 338, is
217 by modulating the activity of *Li*RpiB.
218
219 To facilitate further development of inhibitor leads, a crystal structure for apo *Li*RpiB
220 was determined at 1.6 Å resolution (Table 3). An *Li*RpiB functional dimer was
221 established, and a *Li*RpiB tetramer could then be assembled from the monomer of

the asymmetric unit via crystallographic symmetry (Figure 5). This is similar to the TcRpiB tetramer described by Stern et al (16).

Each monomer of the dimer (hence also of the tetramer) is based on a Rossmann fold with a five-stranded parallel β-sheet flanked by three α-helices on one side and two on the other. A sixth α-helix (C-terminus) extends from the core domain to interact with the second subunit of the dimer. Each monomer subunit of the dimer forms one side of the active site cleft. Within the active site (Figure 6), key residues involved in substrate interaction that have been identified in RpiB homologues are conserved: Asp13, His14, Cys72, Thr74 and Arg116 from one subunit of the dimer and His105, Asn106, Arg140 and Arg144 from the other subunit of the dimer. This indicates the catalytic mechanism operated by the active site is consistent with other RpiBs.

In comparison to the apo *Tc*RpiB structure, a different orientation of Arg 116 (Arg113 in *Tc*RpiB) is observed (Figure 6). Also, Thr74 is present in *Li*RpiB in place of Ser71 that occurs in *Tc*RpiB, more in line with *E. coli* RpiB that also carries a Thr residue at this position (11, 16).

Given the orientation of the sulfate ion in the active site, and the consequent suggestion that the R5P/Ru5P substrate will be oriented in a similar way (Figure 7A), this also indicates 4-PEH interaction with *Li*RpiB will be consistent with that established for other RpiBs (Figure 7B). Docking analysis predictions for anti-parasitic fragment hits 338 and 540 indicates that the interaction of these fragments with the active site are likely to centre around residues His 14, Arg140, Arg144

(Figure 7C and 7D). Given these residues are conserved in RpiB active sites but not RpiAs, this could account for the selectivity of these fragments towards combatting parasites (Table 2).

Discussion

Type B ribose-5-phosphate isomerase (RpiB) has been flagged as an attractive protein target for drug development to combat pathogens, given the critical role of this enzyme combined with its evolutionary divergence from mammalian RpiA. It has long been assumed it may be possible to design RpiB specific inhibitors yet, thus far, no such inhibitors have been identified.

In this work, a fragment library screening was conducted for *L. infantum* RpiB, utilising thermal shift as the screening technique. Thermal shift assaying is commonly used to assess the potential of adding ligands to improve protein stability, aiding crystallization (21, 23, 24). Although not capable of identifying inhibitors directly, it has been widely used to facilitate this process (25–28), assisting in drug discovery efforts. The ability to apply this screening method to any amenable protein, regardless of function, makes thermal shift particularly valuable. This is perhaps most relevant when attempting to establish inhibitors for proteins that lack high-throughput activity-based screening methods, as was the case for *Li*RpiB. Using this method, *Li*RpiB was screened against 851 different fragments. 15 hit fragments that produced ± 5 °C shifts in *Li*RpiB T_m were selected, progressing to *Li*RpiB activity assays and cell viability assays against *L. infantum* parasites. The activity assay results indicate that thermal shift screening was capable of identifying inhibitors as fragments 2, 338, 372, 540 and 576 showed *Li*RpiB inhibitory activity. Significantly, fragment hits 338 and 540 that inhibited *Li*RpiB *in vitro* also displayed anti-parasitic activity towards both *L. infantum* promastigotes (wild-type and *Li*RpiB sKO) and intramacrophagic amastigotes in an infection model, whilst also being well tolerated by mammalian THP1 cells in cytotoxicity assays. Overall, fragment 338 was

276 considered the best hit against *Li*RpiB given its superior potency. The fact that ability
277 to interact with and inhibit *Li*RpiB was utilised to identify anti-parasitic hits
278 strengthens the case for describing *Li*RpiB as a potential chemically validated drug
279 target in *Leishmania infantum*. This is an important observation given the potential
280 value of RpiB as a drug target in parasitic protozoa has formerly been deemed
281 equivocal (6). Though not specifically examined in this study, the fact RpiB is highly
282 conserved amongst *Leishmania* spp. makes it possible these findings could also
283 apply to species beyond *L. infantum*.
284
285 Previous research into RpiB has largely focused on understanding the enzyme's
286 reaction mechanism, particularly in comparison to RpiA, crystal structure elucidation
287 and/or *in silico* docking studies. Notably, in the context of protozoan parasites,
288 although the crystal structure established for *T. cruzi* RpiB has permitted
289 computational ligand docking studies, potential hits have yet to have their anti-
290 parasitic properties confirmed (20). For many years, inhibition of Rpi has centred
291 around the well-established inhibitor 4-PEH. However, low potency and lack of RpiB
292 specificity render this compound inappropriate for chemotherapeutic applications.
293 The inhibitory fragments reported here, several of which were markedly more potent
294 than 4-PEH (1 mM fragment concentration was contrasted with 10 mM 4-PEH
295 inhibitory activity), may be able to fill this void and provide initial scaffolds for
296 structure-led rational optimisation of RpiB inhibitors. In the case of leishmania, the
297 first crystal structures for a leishmanial RpiB, solved during this study, can greatly
298 facilitate this process for *L. infantum* and other *Leishmania* spp..The structural
299 resolution of *Li*RpiB indicates that, as might be anticipated from high levels of protein
300 sequence homology, RpiB structure is highly conserved amongst protozoan

parasites. Thus, there is potential for the design of inhibitors capable of inter-kinetoplastid impact. Docking results for hit anti-parasitic fragments 540 and 338 predict that their interaction with the active site of *Li*RpiB hinges on residues His 14, Arg 140 and Arg 144. These residues typically coordinate the phosphate moiety of substrate R5P, orienting and stabilising the substrate in the correct conformation for isomerisation. Thus, it's possible fragments 540 and 338 compete with R5P in the binding of these key residues. Future co-crystallisation and/or structural modelling of the fragments (and, potentially, further analogues) with *Li*RpiB may shed further light on the RpiB catalytic mechanism but also, crucially, how to gain inhibitor specificity over RpiA. It will also be important to establish how the anti-parasitic fragment hits are turned over by the parasites, as currently speculations can only be made as to how intact fragment compounds could interact with *Li*RpiB.

Furthermore, it is currently unknown whether any off-target effects are also contributing to fragment efficacy, which will be important to determine going forward, as well as anti-parasitic efficacy towards other *Leishmania* spp.. Overall, however, this work provides new avenues to pursue RpiB as a druggable target in *Leishmania* spp. and other pathogenic organisms.

Material and Methods

Cloning of the LiRpiB gene

The *Li*RpiB gene was PCR amplified from *L. infantum* genomic DNA (MHOM/MA/67/ITMAP-263), using the following primers: 5'-CAATTTCCATATGCCGAAGCGTGTTGC-3' and 5'-

CCCAAGCGAATTCTCTACTTTCCTTCC-3'. The purified *Li*RpiB PCR product was NdeI/EcoRI digested and cloned into a pGEM-T Easy vector (Promega). Presence of the *Li*RpiB open-reading frame (ORF) was confirmed via sequencing and was subsequently subcloned into a pET28a(+) expression vector (Novagen).

Expression and purification of recombinant LiRpiB

The pET28a(+) *Li*RpiB expression vector was transformed into *E. coli* BL21 (DE3) cells. The recombinant protein was expressed by induction of log-phase cultures in Luria-Bertani media (O*D600* = 0.6) with 0.5 mM isopropyl-β-D-thiogalactopyranoside (IPTG) for 3 h at 37ºC with shaking at 250 rpm/ min. Bacteria were harvested through centrifugation (3077 g for 40 min at 4ºC) and suspended in 20 mL of buffer A (0.5 M NaCl, 20 mM Tris-HCl, pH 7.6). Samples were then sonicated using a Branson sonifier 250 under the following conditions: output 4, duty cycle 50%, 10 cycles with 15 sec each. Samples were centrifuged (3077 g for 60 min at 4ºC) and the product supernatant was retained for further processing. Recombinant *Li*RpiB was purified in one step using Ni^{2+} resin (ProBond), pre-equilibrated in buffer A. The column was washed sequentially with 2-3 mL of the buffer A, 20 ml of the bacterial crude extract, 2 mL of buffer A 25 mM imidazole, 2 mL of buffer A 30 mM imidazole, 2 x 2 mL of buffer A 40 mM imidazole, 2 mL of buffer A 50 mM imidazole, 10 mL of buffer A 100 mM imidazole, 5 mL of buffer A 500 mM imidazole and 8 ml of buffer B (1 M imidazole, 0.5 M NaCl, 200 mM Tris, pH 7.6). *Li*RpiB enzyme was eluted in the fractions of buffer A containing 100 or 500 mM of imidazole. Desalting was performed against 100 mM of Tris-HCl, pH 7.6 (storage buffer, reaction buffer for direct reaction), using PD-10 Desalting columns (GE Healthcare Code No 17-0851-01).

Differential scanning fluorimetry with LiRpiB

Differential scanning fluorimetry was set up in 96-well PCR plates employing a total reaction volume of 100 µL. Reactions consisted of 13 µM protein (*Li*RpiB) in 50 mM MOPs (pH 8.0) reaction buffer with 5 X SYPRO Orange dye (Invitrogen) as the fluorescent indicator of protein unfolding (Ex. 492 nm, Em. 610 nm). Fragments from an in-house library at the University of St Andrews, expanded from the Maybridge Rule of 3 (Ro3) library (25) were screened against RpiB at 1 mM concentration (0.5% DMSO final concentration per well). This library incorporates fragments that adhere to the chemical parameters ≤ 300 MW; ≤ 3.0 cLogP; ≤ 3 H-bond acceptors; ≤ 3 H-bond donors; ≤ 3 rotatable bonds; ≤ 60 $Å^2$ Polar Surface Area, properties which are predicted to increase the probability of viable fragment lead discovery (29), a more stringent application of the 'Rule of 5' criteria developed by Lipinski et al. to curate drug-like compound libraries (30). DMSO was used in negative control reactions and 30 mM deoxy-ribose-5-phosphate (dR5P) was added to positive control reactions. Each plate screened included 8-replicate negative and 8-replicate positive control reactions, to permit calculation of a Z-factor (31) (threshold = 0.5). Thermal shift scans were performed in a real-time PCR machine (Stratagene Mx3005P with software MxPro v 4.01) over a temperature range of 25°C to 95°C, ramping at 0.5°C min^{-1}. Data were then exported to Excel for analysis using "DSF analysis", modified from the template provided by Niesen et al (21). Melting point (T_m) values were calculated through non-linear regression analysis, fitting the Boltzmann equation to denaturation curves using GraphPad Prism as previously described (25).

Compound preparation for assays

Compounds were dissolved in 100% DMSO at 100 mM, aliquoted and stored at -20°C. The following procedure was applied for the solubilization of compounds in reaction buffer (100 mM Tris-HCl pH 7.6): 1 hour of vortex mixing, 15 minutes of ultrasound treatment and 1 hr of incubation at 37°C under strong agitation. The optical density (OD) at 290 nm of soluble compounds at 1 mM or 0.5 mM concentration was measured and only compounds with low absorbance values (OD < 1) were selected for analysis. The control compound 4-PEH was used as a 100 mM stock in water and stored at -20ºC.

LiRpiB activity assays

Compounds were tested in the forward and/or reverse reaction at a final concentration of 1 mM. Concerning the forward reaction, a direct spectrophotometric method at 290 nm was used to quantify Ru5P formation in the presence of 12.5 mM R5P and 0.0025 mg/ml *Li*RpiB in a total volume of 300 µL (32). The reaction buffer was 100 mM of Tris-HCl pH 7.6. The absorbance was monitored at 37°C for 20 minutes. The blank for each compound was assumed to be the absorbance at *t*=0. Compound inhibitory effect was quantified via measuring OD values in both the presence and absence of compound within the first 4 minutes of the assay and at the endpoint (*t*=20). The ratio between these values were used to determine compound percentage (%) inhibition. In the inverse reaction, a modification of Dische's Cysteine-Carbazole method was used to quantify R5P formation (17). In a total

volume of 15 µL, 5 mM Ru5P, 0.0025 mg/mL *Li*RpiB and 5 µL of compound were incubated for 10 minutes at room temperature. Reaction buffer was 100 mM Tris-HCl, 1 mM EDTA and 0.5 mM 2-mercaptoethanol, pH 8.4. For colour revelation, 15 µL of 0.5% cysteinium chloride, 125 µL of 75% (v/v) sulfuric acid and 5 µl of a 0.1% solution of carbazole in ethanol were added to 10 µl of the previous mixture. The absorbance at 546 nm was determined following incubation for 30 minutes at room temperature in the dark. A blank without enzyme was always run in tandem with and without compound). The enzyme activity in the presence of compounds was measured by subtracting the OD values obtained in the presence of the enzyme to the blank values. Percentage inhibition was assessed via normalization of the activity values against those obtained in the compound negative control reactions.

Parasite culture

L. infantum (MHOM/MA/67/ITMAP-263) wild-type promastigotes and single knockout (sKO) *Li*RpiB promastigotes (19) were maintained at 27ºC in complete RPMI 1640(33). Axenic amastigotes of the same strain expressing firefly luciferase (34) were grown at 37ºC with 5% CO2 in a cell-free medium (35).

Growth inhibition assays

The percentage growth inhibition, in promastigotes was performed by incubating the parasites in a 96-well plate with a starting inoculum of $1x10^6$ cells/ml promastigotes during 72 hours with defined concentrations of the selected fragments. After incubation 50 µM of resazurin was added and incubated for 4 h. Fluorescence was

measured at 540 nm and 620 nm excitation and emission wavelength, respectively, using a Synergy 2 Multi-Mode Reader (Biotek). Activity against intracellular amastigotes was measured using THP1 cells infected with luciferase-expressing amastigotes as previously described (36). Fragments were screened at 100 μM in these assays. THP1 cytotoxicity was determined using an MTT assay following exposure of the THP1 cells to 100 μM of the fragments, as described elsewhere (37).

Production and purification of LiRpiB for crystallization

The purification protocol was based on that of *Tc*RpiB (17). Briefly, full-length *Li*RpiB was produced as described above except that expression was induced overnight at 18°C with 0.7 mM IPTG. Cells were harvested via centrifugation (2500 g for 30 min at 4ºC) and stored at -20°C until use. After thawing, bacterial pellets were suspended in lysis buffer (50 mM Tris.HCl pH 7.5, 300 mM NaCl, 1 mM DTT and 20 mM imidazole). Following sonication, the cell homogenate was centrifuged (56000 g for 30 min at 4ºC) and the soluble tagged protein was purified by affinity chromatography on His60 Ni Superflow Resin (Clontech). Lysis buffer was used to wash the resin and protein was eluted with buffer A (50 mM Tris.HCl pH 7.5, 300 mM NaCl, 1 mM DTT and 500 mM imidazole). After removal of the His-tag (thrombin cleavage - overnight, 4°C), additional SEC was carried out on a HiLoad 16/60 Superdex 200 equilibrated with buffer B (20 mM Tris.HCl pH 7.5, 150 mM NaCl, 2 mM DTT and 1 mM EDTA). Fractions containing purified protein were pooled and protein was concentrated to ~12 mg/ml by ultrafiltration.

Crystallization and data collection

Crystallization experiments were carried out using the sitting drop vapor diffusion method in 96-well plates using an Innovadyne nanodrop robot (300 nl protein solution + 300 nl crystallization condition). *Li*RpiB crystals grew at 277K in 100 mM HEPES (pH 7) and 2 M ammonium sulfate. Crystals were flash-frozen in liquid nitrogen in crystallization condition supplemented with 22% glycerol. Diffraction data were collected on beamline Proxima 1 (SOLEIL, Saclay, France) on a Pilatus 6M detector.

Structure determination and refinement

X-ray data were processed with XDS (38) and the software package CCP4 (39). The *Li*RpiB structure was solved by molecular replacement with Phaser (40, 41) using *Tc*RpiB (Protein Data Bank entry code 3K7O) (16) as the search model. Model building and improvement were conducted by iterative cycles of manual building with Coot (42) and refinement with REFMAC (43). Structural data has been deposited in the Protein Data Bank under entry code 6FXW.

In silico docking analysis

Docking analysis was conducted using PyRx. Ligands (PEH and fragments 338 and 540) were prepared using Chem3D, using the package's MM2 structure optimisation tool. The *Li*RpiB functional dimer was prepared as a macromolecule for docking using AutoDock Tools (44, 45). PyRx docking analysis (46) was performed using a

grid box with dimensions x = 9.217; y = 9.292 and z = 11.459 to encompass the enzyme's active site, determining the ligand conformations that would provide optimal binding energies (exhaustiveness = 16), which were then studied in relation to the *Li*RpiB active site structure using PyMOL.

Acknowledgements

Funding from the European Community's Seventh Framework Programme under grant agreements No. 602773 (Project KINDRED) was received for all partners in this work. This work also received funds from FCT - Fundação para a Ciência e a Tecnologia/Ministério da Ciência, Tecnologia e Ensino Superior through the Research Unit No. 4293 and project POCI-01-0145-FEDER-031013 (PTDC/SAU-PAR/31013/2017 to NS); Individual funding from FCT through SFRH/BD/133485/2017 (to MS) and CEECIND/02362/2017 (to JT).

References

1. James SL, Abate D, Abate KH, Abay SM, Abbafati C, Abbasi N, Abbastabar H, Abd-Allah F, Abdela J, Abdelalim A, Abdollahpour I, Abdulkader RS, Abebe Z, Abera SF, Abil OZ, Abraha HN, Abu-Raddad LJ, Abu-Rmeileh NME, Accrombessi MMK, Acharya D, Acharya P, Ackerman IN, Adamu AA, Adebayo OM, Adekanmbi V, Adetokunboh OO, Adib MG, Adsuar JC, Afanvi KA, Afarideh M, Afshin A, Agarwal G, Agesa KM, Aggarwal R, Aghayan SA, Agrawal S, Ahmadi A, Ahmadi M, Ahmadieh H, Ahmed MB, Aichour AN, Aichour I, Aichour MTE, Akinyemiju T, Akseer N, Al-Aly Z, Al-Eyadhy A, Al-Mekhlafi HM, Al-Raddadi RM, Alahdab F, Alam K, Alam T, Alashi A, Alavian SM, Alene KA, Alijanzadeh M, Alizadeh-Navaei R, Aljunid SM, Alkerwi A, Alla

F, Allebeck P, Alouani MML, Altirkawi K, Alvis-Guzman N, Amare AT, Aminde LN, Ammar W, Amoako YA, Anber NH, Andrei CL, Androudi S, Animut MD, Anjomshoa M, Ansha MG, Antonio CAT, Anwari P, Arabloo J, Arauz A, Aremu O, Ariani F, Armoon B, Ärnlöv J, Arora A, Artaman A, Aryal KK, Asayesh H, Asghar RJ, Ataro Z, Atre SR, Ausloos M, Avila-Burgos L, Avokpaho EFGA, Awasthi A, Ayala Quintanilla BP, Ayer R, Azzopardi PS, Babazadeh A, Badali H, Badawi A, Bali AG, Ballesteros KE, Ballew SH, Banach M, Banoub JAM, Banstola A, Barac A, Barboza MA, Barker-Collo SL, Bärnighausen TW, Barrero LH, Baune BT, Bazargan-Hejazi S, Bedi N, Beghi E, Behzadifar M, Behzadifar M, Béjot Y, Belachew AB, Belay YA, Bell ML, Bello AK, Bensenor IM, Bernabe E, Bernstein RS, Beuran M, Beyranvand T, Bhala N, Bhattarai S, Bhaumik S, Bhutta ZA, Biadgo B, Bijani A, Bikbov B, Bilano V, Bililign N, Bin Sayeed MS, Bisanzio D, Blacker BF, Blyth FM, Bou-Orm IR, Boufous S, Bourne R, Brady OJ, Brainin M, Brant LC, Brazinova A, Breitborde NJK, Brenner H, Briant PS, Briggs AM, Briko AN, Britton G, Brugha T, Buchbinder R, Busse R, Butt ZA, Cahuana-Hurtado L, Cano J, Cárdenas R, Carrero JJ, Carter A, Carvalho F, Castañeda-Orjuela CA, Castillo Rivas J, Castro F, Catalá-López F, Cercy KM, Cerin E, Chaiah Y, Chang AR, Chang HY, Chang JC, Charlson FJ, Chattopadhyay A, Chattu VK, Chaturvedi P, Chiang PPC, Chin KL, Chitheer A, Choi JYJ, Chowdhury R, Christensen H, Christopher DJ, Cicuttini FM, Ciobanu LG, Cirillo M, Claro RM, Collado-Mateo D, Cooper C, Coresh J, Cortesi PA, Cortinovis M, Costa M, Cousin E, Criqui MH, Cromwell EA, Cross M, Crump JA, Dadi AF, Dandona L, Dandona R, Dargan PI, Daryani A, Das Gupta R, Das Neves J, Dasa TT, Davey G, Davis AC, Davitoiu DV, De Courten B, De La Hoz FP, De Leo D, De Neve JW, Degefa MG, Degenhardt L,

526 Deiparine S, Dellavalle RP, Demoz GT, Deribe K, Dervenis N, Des Jarlais DC,
527 Dessie GA, Dey S, Dharmaratne SD, Dinberu MT, Dirac MA, Djalalinia S,
528 Doan L, Dokova K, Doku DT, Dorsey ER, Doyle KE, Driscoll TR, Dubey M,
529 Dubljanin E, Duken EE, Duncan BB, Duraes AR, Ebrahimi H, Ebrahimpour S,
530 Echko MM, Edvardsson D, Effiong A, Ehrlich JR, El Bcheraoui C, El Sayed
531 Zaki M, El-Khatib Z, Elkout H, Elyazar IRF, Enayati A, Endries AY, Er B,
532 Erskine HE, Eshrati B, Eskandarieh S, Esteghamati A, Esteghamati S, Fakhim
533 H, Fallah Omrani V, Faramarzi M, Fareed M, Farhadi F, Farid TA, Farinha
534 CSE, Farioli A, Faro A, Farvid MS, Farzadfar F, Feigin VL, Fentahun N,
535 Fereshtehnejad SM, Fernandes E, Fernandes JC, Ferrari AJ, Feyissa GT, Filip
536 I, Fischer F, Fitzmaurice C, Foigt NA, Foreman KJ, Fox J, Frank TD, Fukumoto
537 T, Fullman N, Fürst T, Furtado JM, Futran ND, Gall S, Ganji M, Gankpe FG,
538 Garcia-Basteiro AL, Gardner WM, Gebre AK, Gebremedhin AT, Gebremichael
539 TG, Gelano TF, Geleijnse JM, Genova-Maleras R, Geramo YCD, Gething PW,
540 Gezae KE, Ghadiri K, Ghasemi Falavarjani K, Ghasemi-Kasman M, Ghimire
541 M, Ghosh R, Ghoshal AG, Giampaoli S, Gill PS, Gill TK, Ginawi IA, Giussani
542 G, Gnedovskaya E V., Goldberg EM, Goli S, Gómez-Dantés H, Gona PN,
543 Gopalani SV, Gorman TM, Goulart AC, Goulart BNG, Grada A, Grams ME,
544 Grosso G, Gugnani HC, Guo Y, Gupta PC, Gupta R, Gupta R, Gupta T,
545 Gyawali B, Haagsma JA, Hachinski V, Hafezi-Nejad N, Haghparast Bidgoli H,
546 Hagos TB, Hailu GB, Haj-Mirzaian A, Haj-Mirzaian A, Hamadeh RR, Hamidi S,
547 Handal AJ, Hankey GJ, Hao Y, Harb HL, Harikrishnan S, Haro JM, Hasan M,
548 Hassankhani H, Hassen HY, Havmoeller R, Hawley CN, Hay RJ, Hay SI,
549 Hedayatizadeh-Omran A, Heibati B, Hendrie D, Henok A, Herteliu C,
550 Heydarpour S, Hibstu DT, Hoang HT, Hoek HW, Hoffman HJ, Hole MK,

551 Homaie Rad E, Hoogar P, Hosgood HD, Hosseini SM, Hosseinzadeh M,
552 Hostiuc M, Hostiuc S, Hotez PJ, Hoy DG, Hsairi M, Htet AS, Hu G, Huang JJ,
553 Huynh CK, Iburg KM, Ikeda CT, Ileanu B, Ilesanmi OS, Iqbal U, Irvani SSN,
554 Irvine CMS, Mohammed S, Islam S, Islami F, Jacobsen KH, Jahangiry L,
555 Jahanmehr N, Jain SK, Jakovljevic M, Javanbakht M, Jayatilleke AU, Jeemon
556 P, Jha RP, Jha V, Ji JS, Johnson CO, Jonas JB, Jozwiak JJ, Jungari SB,
557 Jürisson M, Kabir Z, Kadel R, Kahsay A, Kalani R, Kanchan T, Karami M,
558 Karami Matin B, Karch A, Karema C, Karimi N, Karimi SM, Kasaeian A, Kassa
559 DH, Kassa GM, Kassa TD, Kassebaum NJ, Katikireddi SV, Kawakami N,
560 Kazemi Karyani A, Keighobadi MM, Keiyoro PN, Kemmer L, Kemp GR,
561 Kengne AP, Keren A, Khader YS, Khafaei B, Khafaie MA, Khajavi A, Khalil IA,
562 Khan EA, Khan MS, Khan MA, Khang YH, Khazaei M, Khoja AT, Khosravi A,
563 Khosravi MH, Kiadaliri AA, Kiirithio DN, Kim C Il, Kim D, Kim P, Kim YE, Kim
564 YJ, Kimokoti RW, Kinfu Y, Kisa A, Kissimova-Skarbek K, Kivimäki M, Knudsen
565 AKS, Kocarnik JM, Kochhar S, Kokubo Y, Kolola T, Kopec JA, Kosen S,
566 Kotsakis GA, Koul PA, Koyanagi A, Kravchenko MA, Krishan K, Krohn KJ,
567 Kuate Defo B, Kucuk Bicer B, Kumar GA, Kumar M, Kyu HH, Lad DP, Lad SD,
568 Lafranconi A, Lalloo R, Lallukka T, Lami FH, Lansingh VC, Latifi A, Lau KMM,
569 Lazarus J V., Leasher JL, Ledesma JR, Lee PH, Leigh J, Leung J, Levi M,
570 Lewycka S, Li S, Li Y, Liao Y, Liben ML, Lim LL, Lim SS, Liu S, Lodha R,
571 Looker KJ, Lopez AD, Lorkowski S, Lotufo PA, Low N, Lozano R, Lucas TCD,
572 Lucchesi LR, Lunevicius R, Lyons RA, Ma S, Macarayan ERK, Mackay MT,
573 Madotto F, Magdy Abd El Razek H, Magdy Abd El Razek M, Maghavani DP,
574 Mahotra NB, Mai HT, Majdan M, Majdzadeh R, Majeed A, Malekzadeh R,
575 Malta DC, Mamun AA, Manda AL, Manguerra H, Manhertz T, Mansournia MA,

576 Mantovani LG, Mapoma CC, Maravilla JC, Marcenes W, Marks A, Martins-
577 Melo FR, Martopullo I, März W, Marzan MB, Mashamba-Thompson TP,
578 Massenburg BB, Mathur MR, Matsushita K, Maulik PK, Mazidi M, McAlinden
579 C, McGrath JJ, McKee M, Mehndiratta MM, Mehrotra R, Mehta KM, Mehta V,
580 Mejia-Rodriguez F, Mekonen T, Melese A, Melku M, Meltzer M, Memiah PTN,
581 Memish ZA, Mendoza W, Mengistu DT, Mengistu G, Mensah GA, Mereta ST,
582 Meretoja A, Meretoja TJ, Mestrovic T, Mezerji NMG, Miazgowski B,
583 Miazgowski T, Millear AI, Miller TR, Miltz B, Mini GK, Mirarefin M, Mirrakhimov
584 EM, Misganaw AT, Mitchell PB, Mitiku H, Moazen B, Mohajer B, Mohammad
585 KA, Mohammadifard N, Mohammadnia-Afrouzi M, Mohammed MA,
586 Mohammed S, Mohebi F, Moitra M, Mokdad AH, Molokhia M, Monasta L,
587 Moodley Y, Moosazadeh M, Moradi G, Moradi-Lakeh M, Moradinazar M,
588 Moraga P, Morawska L, Moreno Velásquez I, Morgado-Da-Costa J, Morrison
589 SD, Moschos MM, Mousavi SM, Mruts KB, Muche AA, Muchie KF, Mueller
590 UO, Muhammed OS, Mukhopadhyay S, Muller K, Mumford JE, Murhekar M,
591 Musa J, Musa KI, Mustafa G, Nabhan AF, Nagata C, Naghavi M, Naheed A,
592 Nahvijou A, Naik G, Naik N, Najafi F, Naldi L, Nam HS, Nangia V, Nansseu
593 JR, Nascimento BR, Natarajan G, Neamati N, Negoi I, Negoi RI, Neupane S,
594 Newton CRJ, Ngunjiri JW, Nguyen AQ, Nguyen HT, Nguyen HLT, Nguyen HT,
595 Nguyen LH, Nguyen M, Nguyen NB, Nguyen SH, Nichols E, Ningrum DNA,
596 Nixon MR, Nolutshungu N, Nomura S, Norheim OF, Noroozi M, Norrving B,
597 Noubiap JJ, Nouri HR, Nourollahpour Shiadeh M, Nowroozi MR, Nsoesie EO,
598 Nyasulu PS, Odell CM, Ofori-Asenso R, Ogbo FA, Oh IH, Oladimeji O,
599 Olagunju AT, Olagunju TO, Olivares PR, Olsen HE, Olusanya BO, Ong KL,
600 Ong SK, Oren E, Ortiz A, Ota E, Otstavnov SS, øverland S, Owolabi MO,

Mahesh PA, Pacella R, Pakpour AH, Pana A, Panda-Jonas S, Parisi A, Park EK, Parry CDH, Patel S, Pati S, Patil ST, Patle A, Patton GC, Paturi VR, Paulson KR, Pearce N, Pereira DM, Perico N, Pesudovs K, Pham HQ, Phillips MR, Pigott DM, Pillay JD, Piradov MA, Pirsaheb M, Pishgar F, Plana-Ripoll O, Plass D, Polinder S, Popova S, Postma MJ, Pourshams A, Poustchi H, Prabhakaran D, Prakash S, Prakash V, Purcell CA, Purwar MB, Qorbani M, Quistberg DA, Radfar A, Rafay A, Rafiei A, Rahim F, Rahimi K, Rahimi-Movaghar A, Rahimi-Movaghar V, Rahman M, Ur Rahman MH, Rahman MA, Rahman SU, Rai RK, Rajati F, Ram U, Ranjan P, Ranta A, Rao PC, Rawaf DL, Rawaf S, Reddy KS, Reiner RC, Reinig N, Reitsma MB, Remuzzi G, Renzaho AMN, Resnikoff S, Rezaei S, Rezai MS, Ribeiro ALP, Robinson SR, Roever L, Ronfani L, Roshandel G, Rostami A, Roth GA, Roy A, Rubagotti E, Sachdev PS, Sadat N, Saddik B, Sadeghi E, Saeedi Moghaddam S, Safari H, Safari Y, Safari-Faramani R, Safdarian M, Safi S, Safiri S, Sagar R, Sahebkar A, Sahraian MA, Sajadi HS, Salam N, Salama JS, Salamati P, Saleem K, Saleem Z, Salimi Y, Salomon JA, Salvi SS, Salz I, Samy AM, Sanabria J, Sang Y, Santomauro DF, Santos IS, Santos JV, Santric Milicevic MM, Sao Jose BP, Sardana M, Sarker AR, Sarrafzadegan N, Sartorius B, Sarvi S, Sathian B, Satpathy M, Sawant AR, Sawhney M, Saxena S, Saylan M, Schaeffner E, Schmidt MI, Schneider IJC, Schöttker B, Schwebel DC, Schwendicke F, Scott JG, Sekerija M, Sepanlou SG, Serván-Mori E, Seyedmousavi S, Shabaninejad H, Shafieesabet A, Shahbazi M, Shaheen AA, Shaikh MA, Shams-Beyranvand M, Shamsi M, Shamsizadeh M, Sharafi H, Sharafi K, Sharif M, Sharif-Alhoseini M, Sharma M, Sharma R, She J, Sheikh A, Shi P, Shibuya K, Shigematsu M, Shiri R, Shirkoohi R, Shishani K, Shiue I,

626 Shokraneh F, Shoman H, Shrime MG, Si S, Siabani S, Siddiqi TJ, Sigfusdottir
627 ID, Sigurvinsdottir R, Silva JP, Silveira DGA, Singam NSV, Singh JA, Singh
628 NP, Singh V, Sinha DN, Skiadaresi E, Slepak ELN, Sliwa K, Smith DL, Smith
629 M, Soares Filho AM, Sobaih BH, Sobhani S, Sobngwi E, Soneji SS, Soofi M,
630 Soosaraei M, Sorensen RJD, Soriano JB, Soyiri IN, Sposato LA,
631 Sreeramareddy CT, Srinivasan V, Stanaway JD, Stein DJ, Steiner C, Steiner
632 TJ, Stokes MA, Stovner LJ, Subart ML, Sudaryanto A, Sufiyan MB, Sunguya
633 BF, Sur PJ, Sutradhar I, Sykes BL, Sylte DO, Tabarés-Seisdedos R,
634 Tadakamadla SK, Tadesse BT, Tandon N, Tassew SG, Tavakkoli M, Taveira
635 N, Taylor HR, Tehrani-Banihashemi A, Tekalign TG, Tekelemedhin SW, Tekle
636 MG, Temesgen H, Temsah MH, Temsah O, Terkawi AS, Teweldemedhin M,
637 Thankappan KR, Thomas N, Tilahun B, To QG, Tonelli M, Topor-Madry R,
638 Topouzis F, Torre AE, Tortajada-Girbés M, Touvier M, Tovani-Palone MR,
639 Towbin JA, Tran BX, Tran KB, Troeger CE, Truelsen TC, Tsilimbaris MK, Tsoi
640 D, Tudor Car L, Tuzcu EM, Ukwaja KN, Ullah I, Undurraga EA, Unutzer J,
641 Updike RL, Usman MS, Uthman OA, Vaduganathan M, Vaezi A, Valdez PR,
642 Varughese S, Vasankari TJ, Venketasubramanian N, Villafaina S, Violante FS,
643 Vladimirov SK, Vlassov V, Vollset SE, Vosoughi K, Vujcic IS, Wagnew FS,
644 Waheed Y, Waller SG, Wang Y, Wang YP, Weiderpass E, Weintraub RG,
645 Weiss DJ, Weldegebreal F, Weldegwergs KG, Werdecker A, West TE,
646 Whiteford HA, Widecka J, Wijeratne T, Wilner LB, Wilson S, Winkler AS,
647 Wiyeh AB, Wiysonge CS, Wolfe CDA, Woolf AD, Wu S, Wu YC, Wyper GMA,
648 Xavier D, Xu G, Yadgir S, Yadollahpour A, Yahyazadeh Jabbari SH, Yamada
649 T, Yan LL, Yano Y, Yaseri M, Yasin YJ, Yeshaneh A, Yimer EM, Yip P, Yisma
650 E, Yonemoto N, Yoon SJ, Yotebieng M, Younis MZ, Yousefifard M, Yu C,

651 Zadnik V, Zaidi Z, Zaman S Bin, Zamani M, Zare Z, Zeleke AJ, Zenebe ZM,
652 Zhang K, Zhao Z, Zhou M, Zodpey S, Zucker I, Vos T, Murray CJL. 2018.
653 Global, regional, and national incidence, prevalence, and years lived with
654 disability for 354 Diseases and Injuries for 195 countries and territories, 1990-
655 2017: A systematic analysis for the Global Burden of Disease Study 2017.
656 Lancet 392:1789–1858.
657 2. Dickie EA, Giordani F, Gould MK, Mäser P, Burri C, Mottram JC, Rao SPS,
658 Barrett MP. 2020. New drugs for human African trypanosomiasis: A twenty first
659 century success story. Trop Med Infect Dis 5:1–15.
660 3. World Health Organization. 2020. Leishmaniasis. https://www.who.int/news-
661 room/fact-sheets/detail/leishmaniasis. Accessed: 2020-08-06
662 4. DNDi. 2019. Visceral Leishmaniasis. https://dndi.org/diseases/visceral-
663 leishmaniasis. Accessed: 2020-08-06
664 5. DNDi. 2020. R&D Portfolio. https://dndi.org/research-development/portfolio.
665 Accessed:2020-08-06.
666 6. Kovářová J, Barrett MP. 2016. The Pentose Phosphate Pathway in Parasitic
667 Trypanosomatids. Trends Parasitol 32:622–634.
668 7. Loureiro I, Faria J, Santarem N, Smith TK, Tavares J, Cordeiro-da-Silva A.
669 2018. Potential Drug Targets in the Pentose Phosphate Pathway of
670 Trypanosomatids. Curr Med Chem 25:5239–5265.
671 8. Stincone A, Prigione A, Cramer T, Wamelink MMC, Campbell K, Cheung E,
672 Olin-Sandoval V, Grüning NM, Krüger A, Tauqeer Alam M, Keller MA,
673 Breitenbach M, Brindle KM, Rabinowitz JD, Ralser M. 2015. The return of
674 metabolism: Biochemistry and physiology of the pentose phosphate pathway.
675 Biol Rev 90:927–963.

9. Essenberg MK, Cooper RA. 1975. Two Ribose-5-Phosphate Isomerases from *Escherichia coli* K12: Partial Characterisation of the Enzymes and Consideration of Their Possible Physiological Roles. Eur J Biochem 55:323–332.

10. Capriles PVSZ, Baptista LPR, Guedes IA, Guimaraes ACR, Custodio FL, Alves-Ferreira M, Dardenne LE. 2015. Structural modeling and docking studies of ribose 5-phosphate isomerase from *Leishmania major* and *Homo sapiens*: A comparative analysis for Leishmaniasis treatment. J Mol Graph Model 55:134–147.

11. Zhang RG, Andersson CE, Skarina T, Evdokimova E, Edwards AM, Joachimiak A, Savchenko A, Mowbray SL. 2003. The 2.2 Å resolution structure of RpiB/AlsB from *Escherichia coli* illustrates a new approach to the ribose-5-phosphate isomerase reaction. J Mol Biol 332:1083–1094.

12. Roos AK, Andersson CE, Bergfors T, Jacobsson M, Karlén A, Unge T, Jones TA, Mowbray SL. 2004. *Mycobacterium tuberculosis* ribose-5-phosphate isomerase has a known fold, but a novel active site. J Mol Biol 335:799–809.

13. Roos AK, Mariano S, Kowalinski E, Salmon L, Mowbray SL. 2008. d-Ribose-5-Phosphate Isomerase B from *Escherichia coli* is Also a Functional d-Allose-6-Phosphate Isomerase, While the *Mycobacterium tuberculosis* Enzyme is Not. J Mol Biol 382:667–679.

14. Roos AK, Burgos E, Ericsson DJ, Salmon L, Mowbray SL. 2005. Competitive inhibitors of *Mycobacterium tuberculosis* ribose-5-phosphate isomerase B reveal new information about the reaction mechanism. J Biol Chem 280:6416–6422.

15. Loureiro I, Faria J, Clayton C, Macedo-Ribeiro S, Santarém N, Roy N,

Cordeiro-da-Siva A, Tavares J. 2015. Ribose 5-Phosphate Isomerase B Knockdown Compromises *Trypanosoma brucei* Bloodstream Form Infectivity. PLoS Negl Trop Dis 9:1–11.

16. Stern AL, Naworyta A, Cazzulo JJ, Mowbray SL. 2011. Structures of type B ribose 5-phosphate isomerase from *Trypanosoma cruzi* shed light on the determinants of sugar specificity in the structural family. FEBS J 278:793–808.

17. Stern AL, Burgos E, Salmon L, Cazzulo JJ. 2007. Ribose 5-phosphate isomerase type B from *Trypanosoma cruzi*: kinetic properties and site-directed mutagenesis reveal information about the reaction mechanism. Biochem J 401:279–85.

18. Kaur PK, Tripathi N, Desale J, Neelagiri S, Yadav S, Bharatam P V., Singh S. 2016. Mutational and structural analysis of conserved residues in ribose-5-phosphate isomerase B from *Leishmania donovani*: Role in substrate recognition and conformational stability. PLoS One 11:1–20.

19. Faria J, Loureiro I, Santarem N, Cecilio P, Macedo-Ribeiro S, Tavares J, Cordeiro-da-Silva A. 2016. Disclosing the essentiality of ribose-5-phosphate isomerase B in Trypanosomatids. Sci Rep 6:26937.

20. de V. C. Sinatti V, Luiz LP, Alves-Ferreira M, Dardenne L, Hermínio Martins da Silva J, Guimarães AC. 2017. In silico identification of inhibitors of ribose 5-phosphate isomerase from *Trypanosoma cruzi* using ligand and structure based approaches. J Mol Graph Model 77:168–180.

21. Niesen FH, Berglund H, Vedadi M. 2007. The use of differential scanning fluorimetry to detect ligand interactions that promote protein stability. Nat Protoc 2:2212–21.

22. Hawe A, Sutter M, Jiskoot W. 2008. Extrinsic fluorescent dyes as tools for

protein characterization. Pharm Res 25:1487–1499.

23. Alexandrov AI, Mileni M, Chien EYT, Hanson MA, Stevens RC. 2008. Microscale fluorescent thermal stability assay for membrane proteins. Structure 16:351–9.

24. Ericsson UB, Hallberg BM, DeTitta GT, Dekker N, Nordlund P. 2006. Thermofluor-based high-throughput stability optimization of proteins for structural studies. Anal Biochem 357:289–298.

25. Major LL, Smith TK. 2011. Screening the MayBridge Rule of 3 Fragment Library for Compounds That Interact with the *Trypanosoma brucei* myo-Inositol-3-Phosphate Synthase and/or Show Trypanocidal Activity. Mol Biol Int 2011:389364.

26. Major LL, Denton H, Smith TK. 2013. Coupled Enzyme Activity and Thermal Shift Screening of the Maybridge Rule of 3 Fragment Library Against *Trypanosoma brucei* Choline Kinase; A Genetically Validated Drug Target, p. 413–431. *In* El-Shemy, HA (ed.), Drug Discovery. InTech.

27. Lo M-C, Aulabaugh A, Jin G, Cowling R, Bard J, Malamas M, Ellestad G. 2004. Evaluation of fluorescence-based thermal shift assays for hit identification in drug discovery. Anal Biochem 332:153–9.

28. Krishna SN, Luan CH, Mishra RK, Xu L, Scheidt KA, Anderson WF, Bergan RC. 2013. A fluorescence-based thermal shift assay identifies inhibitors of mitogen activated protein kinase kinase 4. PLoS One 8.

29. Carr RAE, Congreve M, Murray CW, Rees DC. 2005. Fragment-based lead discovery: Leads by design. Drug Discov Today 10:987–992.

30. Lipinski CA, Lombardo F, Dominy BW, Feeney PJ. 1997. Experimental and computational approaches to estimate solubility and permeability in drug

751 discovery and development settings. Adv Drug Deliv Rev 23:3–25.
752 31. Zhang J-H, Chung TDY, Oldenburg KR. 1999. A Simple Statistical Parameter
753 for Use in Evaluation and Validation of High Throughput Screening Assays. J
754 Biomol Screen 4:67–73.
755 32. Igoillo-Esteve M, Maugeri D, Stern a L, Beluardi P, Cazzulo JJ. 2007. The
756 pentose phosphate pathway in *Trypanosoma cruzi*: a potential target for the
757 chemotherapy of Chagas disease. An Acad Bras Cienc 79:649–663.
758 33. Moreira D, Santarém N, Loureiro I, Tavares J, Silva AM, Amorim AM, Ouaissi
759 A, Cordeiro-da-Silva A, Silvestre R. 2012. Impact of continuous axenic
760 cultivation in *Leishmania infantum* virulence. PLoS Negl Trop Dis 6:e1469.
761 34. Sereno D, Roy G, Lemesre JL, Papadopoulou B, Ouellette M. 2001. DNA
762 transformation of *Leishmania infantum* axenic amastigotes and their use in
763 drug screening. Antimicrob Agents Chemother 45:1168–73.
764 35. Sereno D, Lemesre JL. 1997. Axenically cultured amastigote forms as an in
765 vitro model for investigation of antileishmanial agents. Antimicrob Agents
766 Chemother 41:972–6.
767 36. Santarém N, Tavares J, Cordeiro-da-Silva A. 2019. In Vitro Infections of
768 Macrophage-Like Cell Lines with *Leishmania infantum* for Drug Screening, p.
769 265–277. *In* .
770 37. Linciano P, Dawson A, Pöhner I, Costa DM, Sá MS, Cordeiro-da-Silva A,
771 Luciani R, Gul S, Witt G, Ellinger B, Kuzikov M, Gribbon P, Reinshagen J, Wolf
772 M, Behrens B, Hannaert V, Michels PAM, Nerini E, Pozzi C, di Pisa F, Landi
773 G, Santarem N, Ferrari S, Saxena P, Lazzari S, Cannazza G, Freitas-Junior
774 LH, Moraes CB, Pascoalino BS, Alcântara LM, Bertolacini CP, Fontana V,
775 Wittig U, Müller W, Wade RC, Hunter WN, Mangani S, Costantino L, Costi MP.

2017. Exploiting the 2-Amino-1,3,4-thiadiazole Scaffold To Inhibit *Trypanosoma brucei* Pteridine Reductase in Support of Early-Stage Drug Discovery. ACS omega 2:5666–5683.

38. Kabsch W. 2010. XDS. Acta Crystallogr Sect D Biol Crystallogr 66:125–132.

39. Winn MD, Ballard CC, Cowtan KD, Dodson EJ, Emsley P, Evans PR, Keegan RM, Krissinel EB, Leslie AGW, McCoy A, McNicholas SJ, Murshudov GN, Pannu NS, Potterton EA, Powell HR, Read RJ, Vagin A, Wilson KS. 2011. Overview of the CCP 4 suite and current developments. Acta Crystallogr Sect D Biol Crystallogr 67:235–242.

40. Collaborative Computational Project N 4. 1994. The CCP4 suite: programs for protein crystallography. Acta Crystallogr D Biol Crystallogr 50:760–3.

41. McCoy AJ, Grosse-Kunstleve RW, Adams PD, Winn MD, Storoni LC, Read RJ. 2007. Phaser crystallographic software. J Appl Crystallogr 40:658–674.

42. Emsley P, Lohkamp B, Scott WG, Cowtan K. 2010. Features and development of Coot. Acta Crystallogr D Biol Crystallogr 66:486–501.

43. Murshudov GN, Skubák P, Lebedev AA, Pannu NS, Steiner RA, Nicholls RA, Winn MD, Long F, Vagin AA. 2011. REFMAC 5 for the refinement of macromolecular crystal structures. Acta Crystallogr Sect D Biol Crystallogr 67:355–367.

44. Sanner MF. 1999. Python: a programming language for software integration and development. J Mol Graph Model 17:57–61.

45. Morris GM, Huey R, Lindstrom W, Sanner MF, Belew RK, Goodsell DS, Olson AJ. 2009. AutoDock4 and AutoDockTools4: Automated docking with selective receptor flexibility. J Comput Chem 30:2785–91.

46. Dallakyan S, Olson AJ. 2015. Small-Molecule Library Screening by Docking

with PyRxMethods in Molecular Biology.

Figure Legends

Figure 1 – Overview of the pentose phosphate pathway (PPP). Both oxidative and non-oxidative branches of the pathway are depicted. Ribose-5-phosphate isomerase (Rpi) is highlighted in bold. G6PDH – glucose-6-phosphate dehydrogenase; 6-PGL; 6-phosphogluconolactonase; 6-PGDH – 6-phosphogluconate dehydrogenase; RuPE – Ribulose 5-phosphate epimerase; TKT– transketolase; TAL – transaldolase.

Figure 2: Confirmation *Li*RpiB is amenable to thermal shift library screening. Fluorescence profiles for 8 replicate *Li*RpiB negative control reactions (protein in the absence of any potential ligand) and 8 replicate positive control reactions (*Li*RpiB in the presence of 30 mM dR5P) are shown. LiRpiB T_m = 59.3 ± 0.08 °C**.** The presence of 30 mM dR5P produced a 6 °C T_m shift (*Li*RpiB T_m = 65.6 ± 0.11 °C).

Figure 3: Measurements of *Li*RpiB activity catalysing the forward reaction in the presence of the fragment 576. Values represent the enzyme activity with (squares) and without (circles) the fragment, and with 4-PEH (triangles). The reaction occurred in the presence of 12.5 mM R5P and 0.0025 mg/ml *Li*RpiB. Fragment 576 and 4-PEH were tested at 1 mM and 10 mM respectively. The absorbance at 290 nm (OD)

826 was measured every 30 seconds during 20 minutes at 37°C. The values obtained
827 with the compound 576 and in the control without the fragment correspond to the
828 mean of duplicates. The values concerning the 4-PEH were obtained from a single
829 enzymatic kinetic reading.

830 Figure 4: Average dose response curves. EC50 and 95% confidence interval for
831 miltefosine (A) and fragment 338 (B) anti-parasitic activity against wild-type (WT) and
832 single knockout (sKO) RpiB promastigotes. The curves represent the merged output
833 from the data of three independent curves.
834
835 Figure 5: Reconstitution of *Li*RpiB structure. The green monomer represents the
836 asymmetric unit and additional copies participating in tetramer formation through
837 crystallographic symmetry are depicted in grey.
838
839 Figure 6: *Li*RpiB active site occupied by a sulfate ion. Key residues for *Li*RpiB protein
840 activity are labelled and depicted as sticks, water molecules as red spheres.
841 Conformation of *Tc*RpiB Arg113, as observed in the *Tc*RpiB apo structure, is
842 highlighted in brown transparent stick.
843
844 Figure 7 – *Li*RpiB active site illustrating inhibitor substrate and inhibitor binding
845 predictions. (A) R5P/Ru5P and (B) 4-PEH, predicted with reference to *Tc*RpiB; (C)
846 338 and (D) 540 fragment binding predictions from *in silico* docking analysis. The
847 docking conformations depicted displayed optimal binding energy and highest level
848 of intermolecular interactions.
849

850 Table 1: Fragment hits from thermal shift screening of *Li*RpiB. Fragment library

851 number; name; chemical structure and observed T_m shift (°C) for each fragment hit

852 are provided.

853

Fragment ID	Name	Structure	T_m shift (°C)
2	pyridin-4-amine	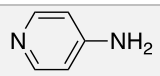	12.9
3	pyrrolidine-1-carbonitrile	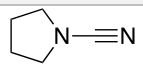	5.8
25	2-ethyl-4-methyl-1H-imidazole	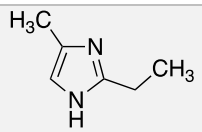	7.4
68	2-aminothiophene-3-carbonitrile	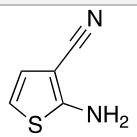	-9.2
152	quinolin-2-amine	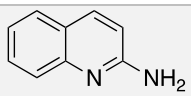	6.6
278	(1-methyl-1H-indol-6-yl)methanol	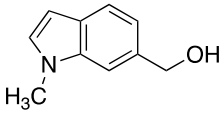	5.6
328	4H-thieno[3,2-b]pyrrole-5-carboxylic acid	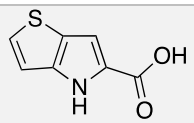	10.4
338	3-(2-furyl)benzonitrile	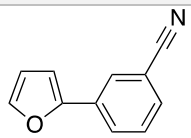	5.8
372	[4-(1H-pyrrol-1-yl)phenyl]methanol	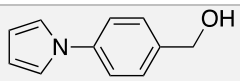	6.9
383	[4-(2-furyl)phenyl]methanol	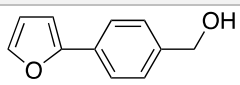	9.7
458	[5-(2-furyl)thien-2-yl]methanol	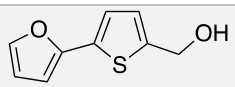	7.6
540	(5-phenoxy-2-furyl)methanol	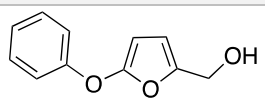	6.5
565	4-(2-amino-1,3-thiazol-4-yl)phenol	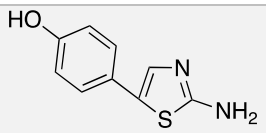	-8.2
576	2,4-difluorobenzenesulfonamide	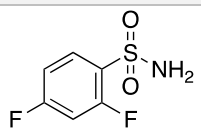	-8.7

Antimicrobial Agents and Chemotherapy

626	1,3-benzothiazol-2-ylmethylamine hydrochloride	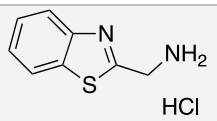	-6.9

Table 2: Inhibitory capacity of compounds against *Li*RpiB

The enzymatic inhibition of all the compounds was determined at 1 mM, except the 4-PEH that was tested at 10 mM. The values correspond to the mean +/- SD of the inhibitory effect (%) relative to control (drug absence) from 2-3 independent assays performed in duplicate. The activity of 100 µM of each fragment against *L. infantum* promastigotes was determined using resazurin assay (72 hours). For the intra-macrophagic parasites, THP1 cells infected with parasites expressing luciferase were used. The cytotoxicity and activity determinations were performed with 100 µM of the fragments in a MTT assay involving PMA-differentiated THP-1 cells. Anti-parasite and viability data represented is the average ± SD of at least two independent assays performed in at least triplicate. NA, not active; NT, not tested.

Inhibitor	*Li*RpiB inhibition (%)		Anti-parasitic activity (%)			THP1 viability (%)
	Forward	Reverse	Promastigote WT	Promastigote sKO RpiB	Amastigote	
2	10 ± 14	21 ± 2	N.A.	N.A.	30 ± 8	92 ± 1
3	12 ± 9	10 ± 4	14 ± 5	9 ± 0	79 ± 26	99 ± 3
25	6 ± 1	6 ± 7	N.A.	N.A.	40 ± 31	115 ± 26
68	N.T.	19 ± 1	N.A.	N.A.	N.A.	120 ± 18
152	N.T.	13 ± 8	31 ± 11	52 ± 24	N.A.	114 ± 15
278	N.T.	4 ± 4	13 ± 1	28 ± 5	N.A.	19 ± 1
338	N.T.	32 ± 10	100 ± 0	102 ± 2	100 ± 17	77 ± 14
372	5 ± 15	26 ± 3	N.A.	N.A.	N.A.	96 ± 5
383	N.T.	-2 ± 1	N.A.	N.A.	N.A.	121 ± 16
540	N.T.	23 ± 5	26 ± 15	64 ± 5	87 ± 15	71 ± 2
565	N.T.	17 ± 1	N.A.	N.A.	N.A.	96 ± 0
576	39 ± 22	14 ± 5	N.A.	69 ± 28	N.A.	21 ± 20
626	N.T.	-7 ± 8	N.A.	N.A.	N.A.	101 ± 4
4PEH	51 ± 19	24 ± 4	N.A.	N.A.	N.A.	82 ± 1

Table 3. Data collection and refinement statistics

	*Li*RpiB/SO_4
Data collection	

Resolution (last shell) (Å)	19.75-1.57 (1.66-1.57)
Space group	F222
Unit-cell parameters a, b, c (Å) α, β, γ (°)	 a=80.87, b=83.55, c=89.35 α=β=γ=90
Completeness (last shell) (%)	99.6 (97.8)
Redundancy (%)	6.5
I/σ(I) (last shell)	23.20 (5.09)
Rsym(I) (last shell) (%)	5.27(34.3)
Refinement	
Protein molecule / A.U.	1
R_{work} (%)	14.5
R_{free} (%)	17.8
r.m.s.d. in bond lengths (Å)	0.024
r.m.s.d. in bond angles (°)	2.217
Mean B factors (Å^2)	17.35
PDB entry code	6FXW

868

869

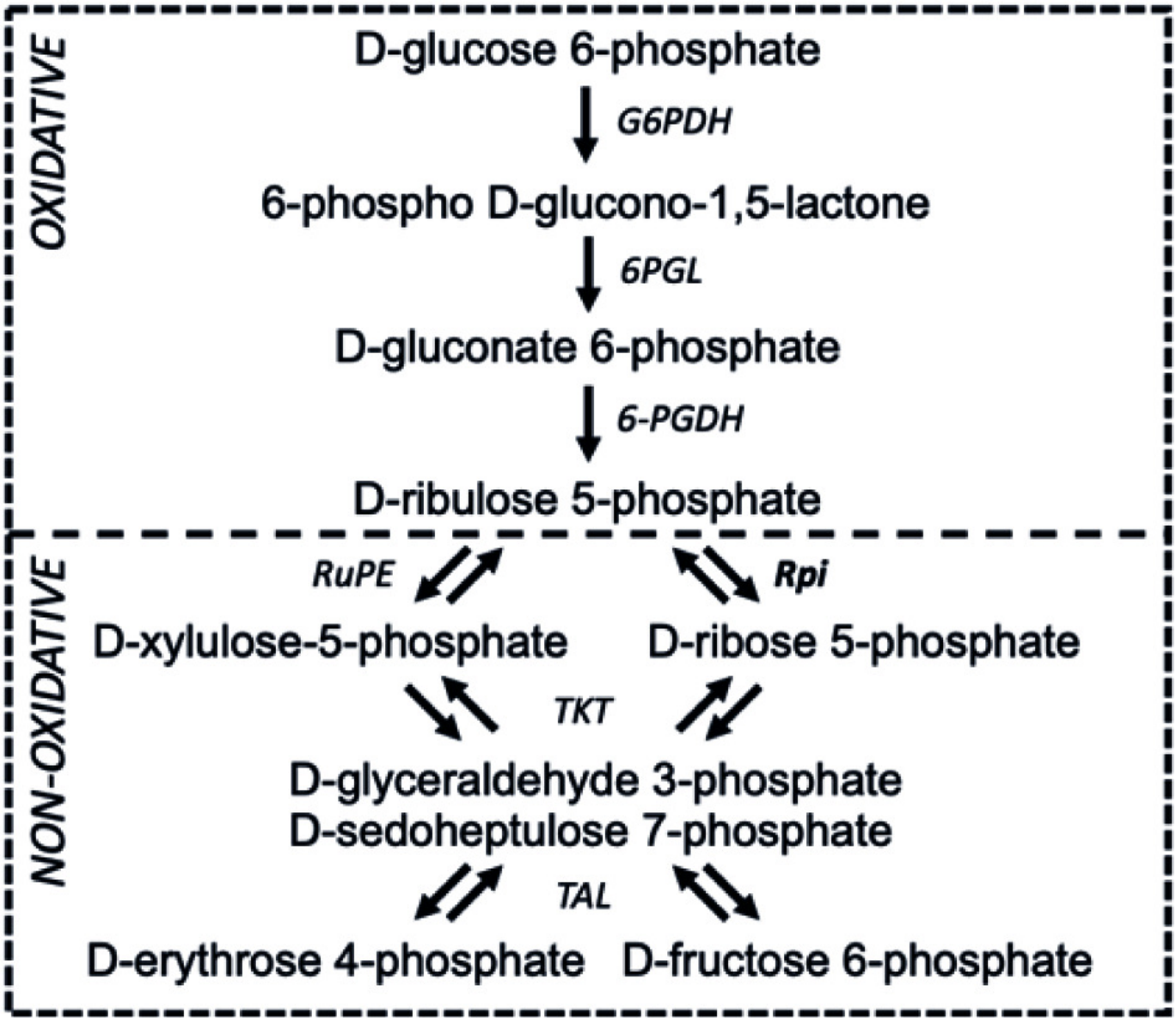

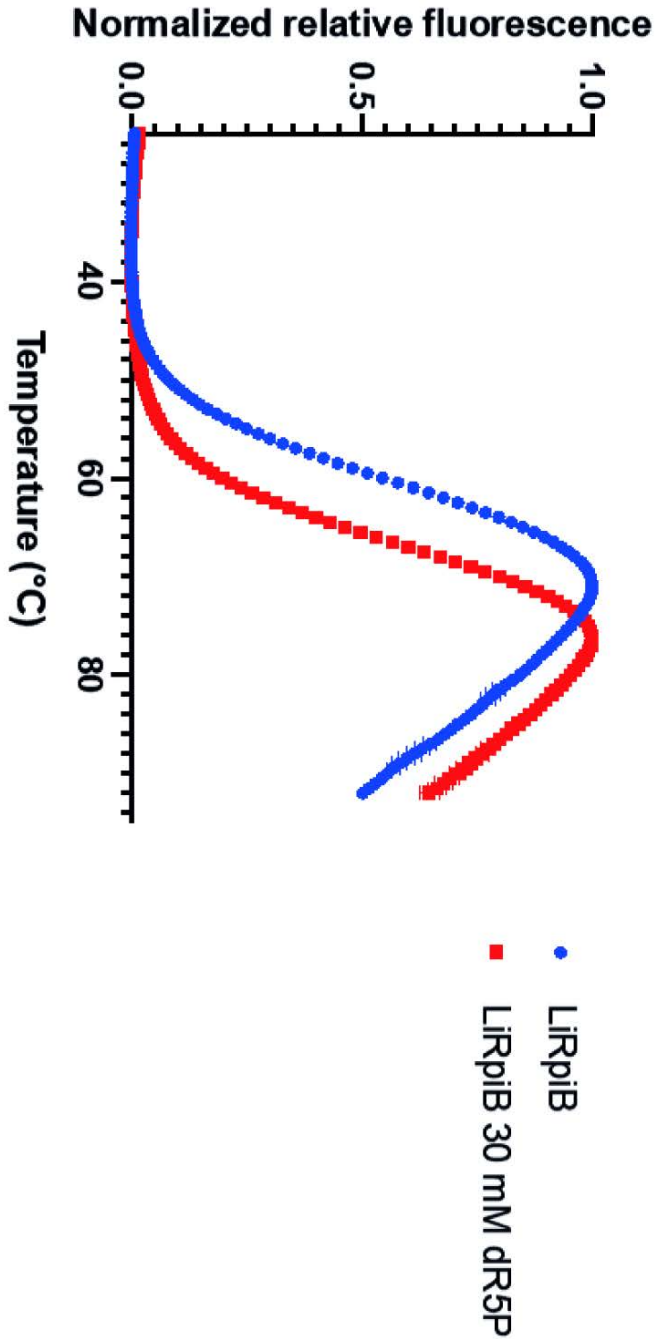

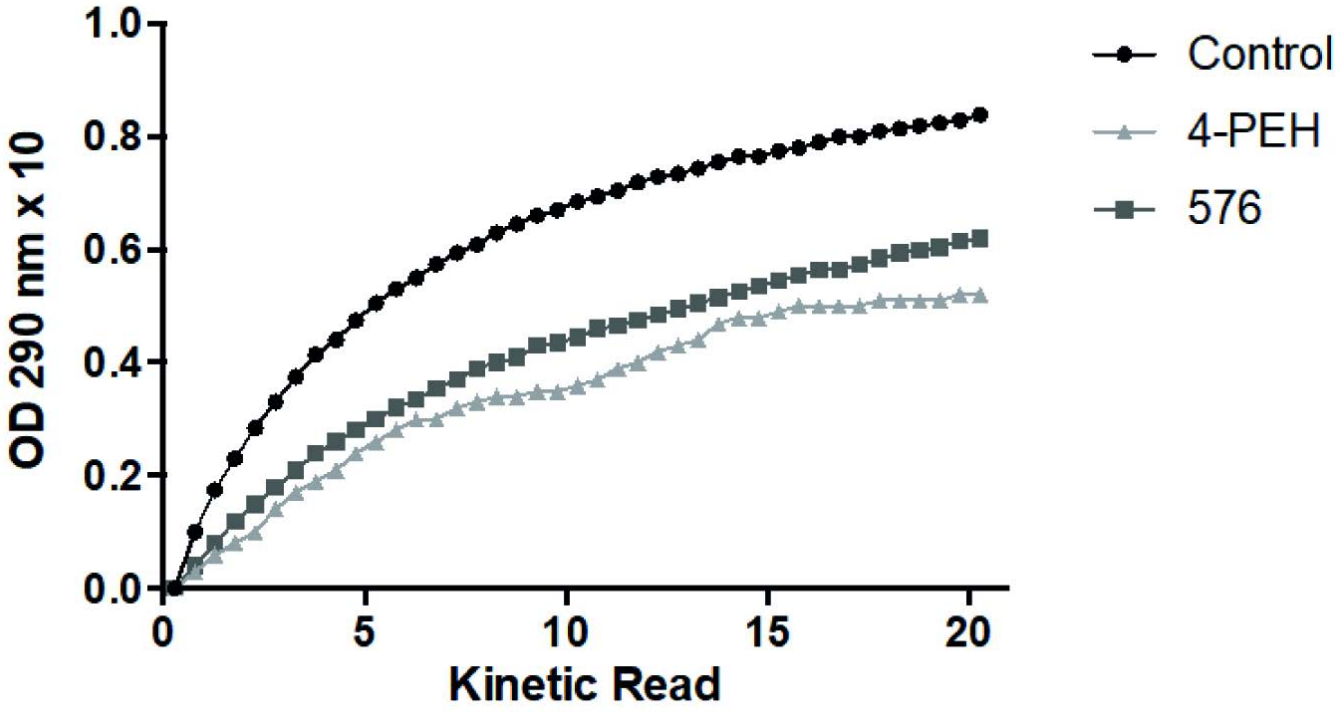

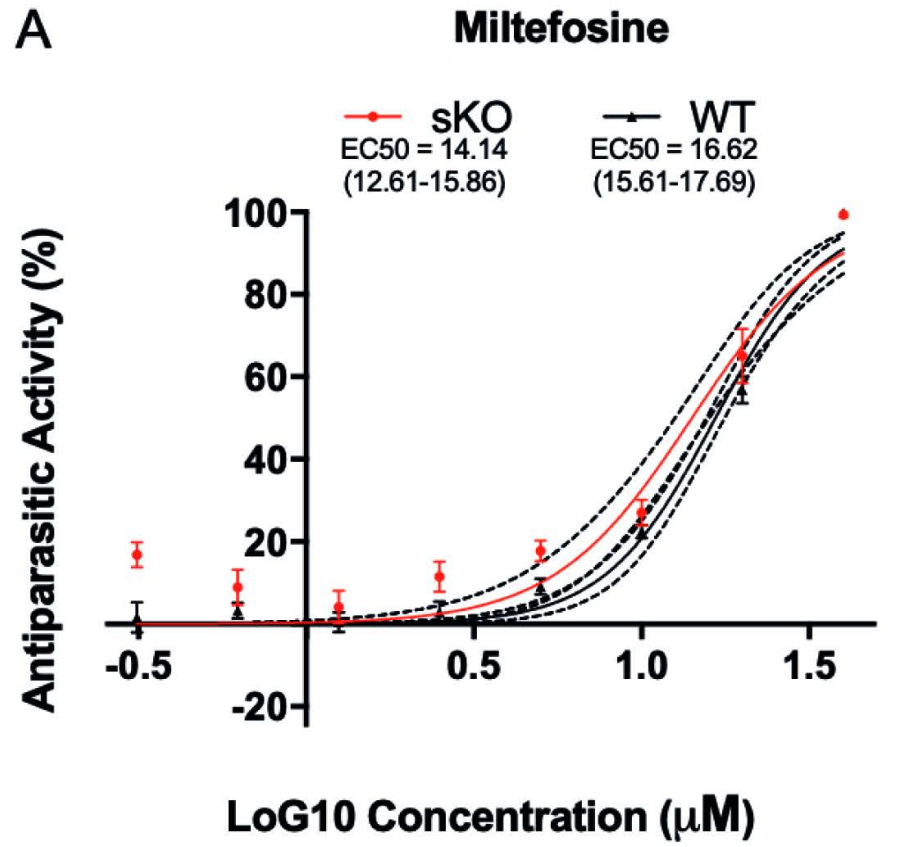

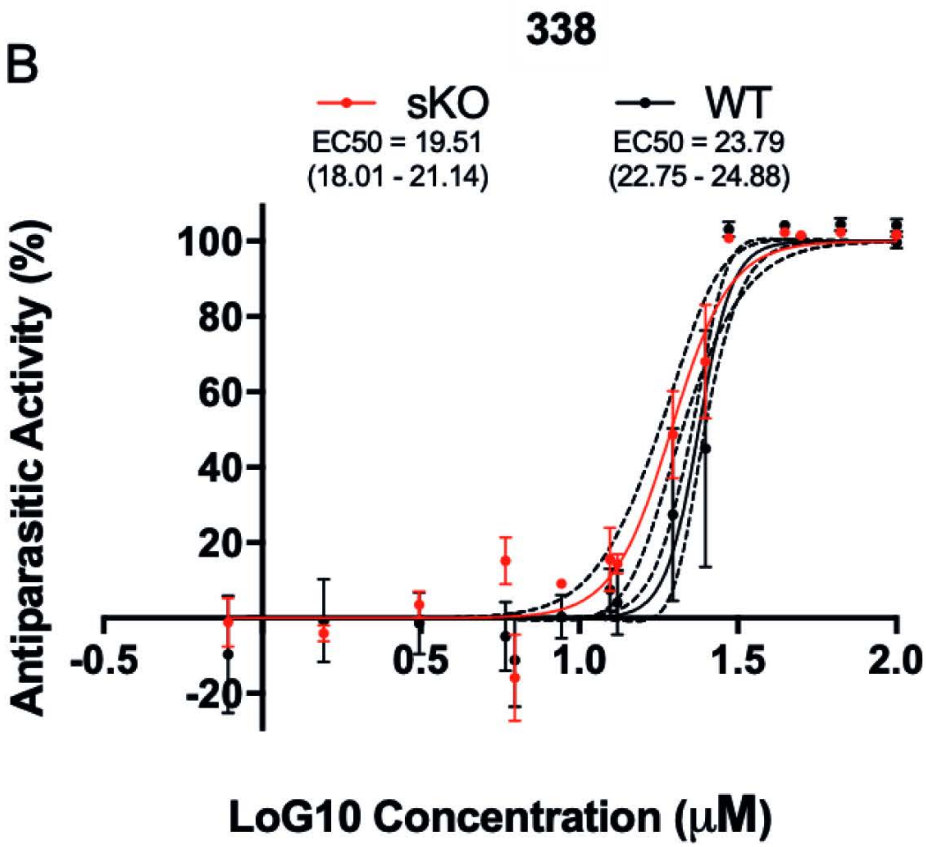

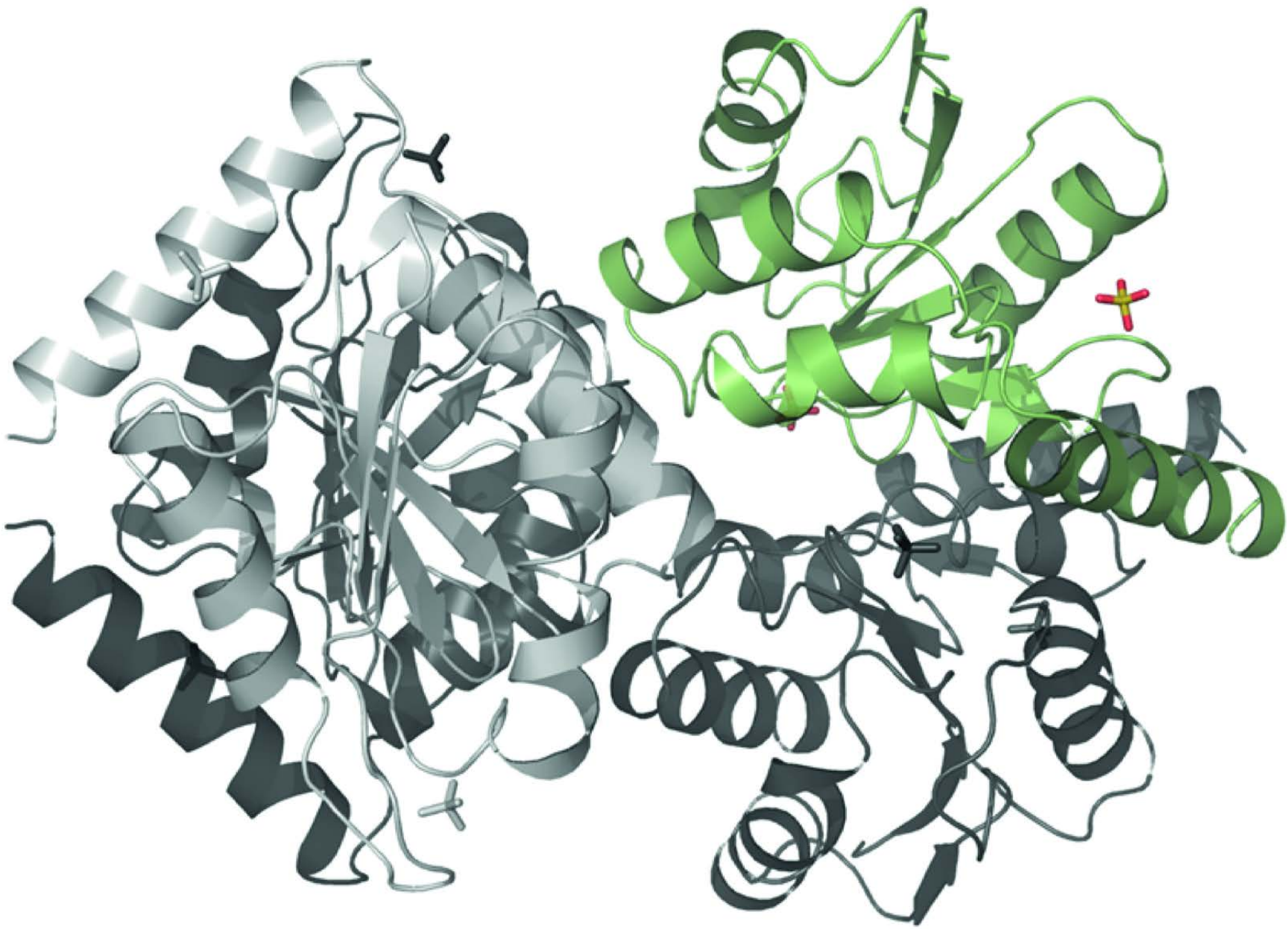

Antimicrobial Agents and Chemotherapy
AAC
Antimicrobial Agents and Chemotherapy